Advances in Aircraft and Spacecraft Science, *Vol. 4, No. 6 (2017) 651-677*
DOI: https://doi.org/10.12989/aas.2017.4.6.651

Determination of taxiing resistances for transport category airplane tractive propulsion

Nihad E. Daidzic*[1,2]

[1]*AAR Aerospace Consulting, LLC, P.O. Box 208 Saint Peter, MN 56082-0208, USA*
[2]*Minnesota State University, Mankato, MN 56001, USA*

(Received June 4, 2017, Revised July 1, 2017, Accepted July 2, 2017)

Abstract. For the past ten years' efforts have been made to introduce environmentally-friendly "green" electric-taxi and maneuvering airplane systems. The stated purpose of e-taxi systems is to reduce the taxiing fuel expenses, expedite pushback procedures, reduce gate congestion, reduce ground crew involvement, and reduce noise and air pollution levels at large airports. Airplane-based autonomous traction electric motors receive power from airplane's APU(s) possibly supplemented by onboard batteries. Using additional battery energy storages ads significant inert weight. Systems utilizing nose-gear traction alone are often traction-limited posing serious dispatch problems that could disrupt airport operations. Existing APU capacities are insufficient to deliver power for tractive taxiing while also providing for power off-takes. In order to perform comparative and objective analysis of taxi tractive requirements a "standard" taxiing cycle has been proposed. An analysis of reasonably expected tractive resistances has to account for steepest taxiway and runway slopes, taxiing into strong headwind, minimum required coasting speeds, and minimum acceptable acceleration requirements due to runway incursions issues. A mathematical model of tractive resistances was developed and was tested using six different production airplanes all at the maximum taxi/ramp weights. The model estimates the tractive force, energy, average and peak power requirements. It has been estimated that required maximum net tractive force should be 10% to 15% of the taxi weight for safe and expeditious airport movements. Hence, airplanes can be dispatched to move independently if the operational tractive taxi coefficient is 0.1 or higher.

Keywords: airplane taxiing resistances; traction taxiing; electric taxiing; traction force; energy, and power; aerodynamic drag in the ground effect; wind resistance; tire dynamics; airport design

1. Introduction

Airport operations leave significant negative footprint on the local environment. Of the main environmental pollutants at the airports, noise and air pollution are principal (Hershey and Turner 1974, Ignaccolo 2000, Kuznetsov 2003, Vanker *et al.* 2009, Page and Hobbs 2010, Mirosavljević *et al.* 2011, Heleno *et al.* 2014). While the negative effect of air pollution on human health is obvious, well documented, and understood, it is even asserted that there is a correlation between the airport noise and cardiovascular diseases (Stansfeld 2013). Treatment of aircraft jet engine and airport noise is given in, more or less detail, Kerrebrock (1992), and Filippone (2012).

*Corresponding author, Professor, E-mail: Nihad.Daidzic@aaraerospacecon.com

http://www.techno-press.org/?journal=aas&subpage=7 ISSN: 2287-528X (Print), 2287-5271 (Online)

Additionally, large amount of fuel is used during prolonged taxi operations and often delayed departures with jet engines idling. It is estimated that about 32 million commercial air transportation operations occurred world-wide in 2015 (IATA 2016). Every cycle will involve one taxi-out and takeoff and one landing and taxi-in with the total average taxi distance of 4 NM per cycle. That would be about 128 million NM (237 million km) of ground taxi operations/maneuvering annually (in 2015) and does not include GA operations.

Attempts are currently underway to introduce alternative taxiing methods. Electric traction prime movers are typically proposed which is in line with the trends toward the More Electric Airplane (MEA) designs (Moir and Seabridge 2008). Recently, Hospodka (2014) examined three proposed electrical taxi drive systems: Wheeltug (company registered in Gibraltar), EGTS (Honeywell/Safran), and Taxibot (IAI). Wheeltug system apparently only powers nose-gear (NG) wheels and may be applicable only to smaller T-category airplanes. The EGTS system uses traction motors in main-gear (MG) wheels. The electric power for traction electric motors (e-motors) is supplied by aircraft Auxiliary Power Units (APUs). The problem with the onboard electrical taxi drive systems being currently tested is that APU generated electrical power alone is not sufficient to reliably meet taxi traction resistances (Hospodka 2014). The most modern T-category MEAs (B787, A380, etc.), the maximum electrical power production is on the order of one MW (1,340 HP), but only with all engines and associated AC generators operating. Their respective APU's cannot deliver sufficient power for tractive taxiing. Large part of the APU power production is needed to run pressurization, air-packs and other ground services. For example, A380 uses two 120 kVA constant-frequency (CF) 400 Hz 115 VAC APUs, while B787 has two 225 kVA APU starter/generators (Wild 2008, Moir and Seabridge 2008, 2013). A B767-300ER uses one 90 kVA CF 400 Hz 115 VAC APU, which supplies necessary electrical power and pneumatic air for pressurization and A/C, while the main engines are off. In another example, the Brazilian-manufactured Embraer 190/195 model uses speed-governed turboshaft APU with a CF generator producing maximum 40 kVA at a standard 400 Hz three-phase 115/200 VAC (Freitas and Daidzic 2017). Existing aircraft APUs are, in general, grossly underpowered to provide required muscle for traction motors even at their full capacity. Additionally, APUs are indeed turboshaft engines which use hydrocarbon (HC) jet fuels. Having more powerful onboard APUs being able to generate enough power for electrical traction motors only partially resolves the issue of airport air pollution, noise, and excessive HC fuel consumption due to taxi maneuvering.

Electrical traction motors located only in NG, while very attractive idea, cannot provide reliably required taxi traction in all operational instances due to airplane's design low NG vertical loading. For example, only about 6-10% weight is supported by the nose gear during taxiing. The NG loading will depend on the exact center of gravity/mass (CG/CM) location, or more commonly, expressed in the T-category airplane operations on the MAC (Mean Aerodynamic Chord) setting. For example, an A320-200 weighing about 172,000 lb on the ramp and in a typical seating configuration will bear about 13,800 lbf (61.39 kN) vertical load on the retractable NG assembly. If the taxi surface is wet and smooth with the associated coefficient of tractive friction (CTF) of 0.5, the traction limit becomes 6,900 lbf (30.69 kN). Maximum sustained grade that could be negotiated with rolling resistance is about 3%, but at a crawling speed, no headwind (HW), no aero-drag, and no tractive reserve for even faintest acceleration. Any attempt to accelerate, even gently, may result in NG tire(s) slip. Similar conclusions were made by Teo *et al.* (2008) and more recently by Hospodka (2014). Such disabled aircraft would be unacceptable in daily airport operations. Additionally, too slow taxi speeds could cause congestions, collision hazards, delays, and significantly impact operations. Electronic traction control, such as in

automotive applications (Braess and Seifert 2005), would be required for efficient traction taxi, just as fully-modulated anti-skid systems are required for airplane brakes.

The status of the EGTS system by Honeywell and Safran is currently unknown with announced delays. Taxibot system is remotely controlled by airplane flight crew, but may be impractical for other reasons and at the end it is not that much different than the existing ground tow trucks (albeit without drivers). It is in fact a self-driving and/or remotely-controlled tug which may cause congestion and collision hazard at busy airports when returning back to gates. After landing an airplane will have to wait for respective Taxibot unit to arrive and get hooked up, which may cause operational delays and collision hazards. On the other hand, Taxibot units (800-1,500 HP) are not as much power-limited. However, diesel-powered tow trucks also generate noise and air pollution and use HC fuels. In the opinion of this author it would be best to have autonomous independent airplane tractive taxiing drive and not rely on external tow trucks/tugs. Autonomous taxiing traction systems should be capable of reverse mode to pull the airplane back from the gate. Using wide-angle rear-view cameras with display on multi-functional-displays (MFDs), the flight crew can independently control and supervise push-back operations with the ground personnel only monitoring. Additional functionality of tractive motors may be in pre-rotating tires for landing and providing for regenerative braking (RB).

Before tractive taxiing energy, power, torques, and tractive force requirements can be specified it is important to estimate taxiing resistances for various aircraft. Hence, a detailed mathematical model of airplane taxiing resistances was developed. Traction requirements were established using, here developed, "standard" taxi cycle. We are not aware of any regulatory or recommended taxiing cycle/schedule. Driving cycles (schedules) are well known, measured, and available for road vehicles (Morlok 1978, Miller 2004, Braess and Seifert 2005, Larminie and Lowry 2012), but nothing was found for taxiing airplanes. If such taxiing system is implemented in the future on large scales perhaps special ATC taxi procedures would need to be developed to define boundaries of traction-taxiing zones before departure and after landings.

Very little exists in the public domain regarding alternative taxiing systems. The only article we found specifically targeting this topic was by Teo *et al.* (2008). Unfortunately, no methodology and no working equations were provided and so it is difficult to verify the results. There also seem to be some confusion between slopes in degrees and percentages. Nevertheless, some pertinent conclusions and observations were made regarding the NG and the MG traction systems and requirements. A recent US patent on e-taxi solution was issued to Hughes *et al.* (2013). Recently Hospodka (2014) in an aviation industry magazine compared three novel e-taxi systems and also concluded that NG traction may be too limiting, especially for the larger T-category airplanes. The author then mostly focused on Taxibot systems with associated cost and performance.

The intent of this article is to propose standardization of taxi cycles (schedules) with the purpose of reliably estimating and comparing driving resistances for a wide variety of T-category airplane models. Furthermore, the goal is to establish realistic traction force, energy, and power requirements for safe, dependable, and expedited airport operations of future independent traction taxi systems.

2. Mathematical model of airplane taxiing resistances

An airplane using NG and/or MG wheel/tires tractive propulsion is not that much different from road vehicles. In the subsequent dynamic analysis, it is assumed that the main propulsive

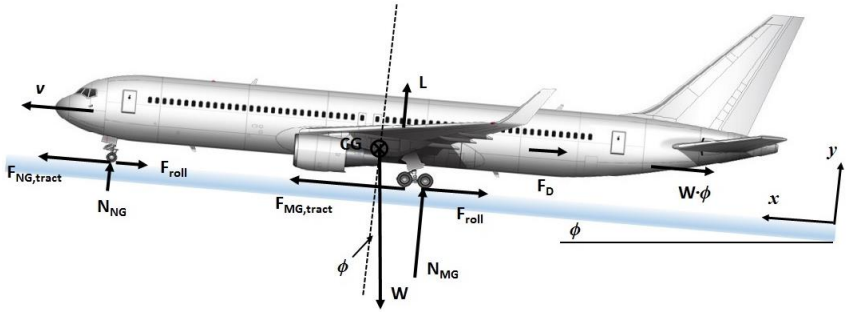

Fig. 1 Forces acting on an airplane taxiing on upsloped TWY with the propulsive force coming solely from the nose-gear and selected main-gear traction units. Not to scale

(jet) engines are not generating any forward thrust. The main forces acting on the airplane are the traction propulsion from the NG and/or MG tires and various resistances including the gravity retardation from upslope taxiways (TWYs) or runways (RWYs), tire rolling resistance force expressed through the coefficient of rolling resistance (CRR), and the aerodynamic drag in the presence of steady HW as adverse condition. The highest translational driving resistance normally comes from the inertial (acceleration) forces. An illustration of a T-category airplane taxiing and main forces is shown in Fig. 1.

2.1 Equations of external taxiing resistances

Using the 2nd Newtonian Law of classical mechanics in sufficiently inertial flat-Earth topocentric frame of reference fixed at the airport in consideration, one can write the external or net resistances for a differential lumped-parameter uni-directional (x-component only) airplane motion

$$M_{eff}\cdot a = M_A\cdot\kappa\cdot\frac{dv}{dt} = \underbrace{\left[F_{NG,tract}(v)+F_{MG,tract}(v)\right]}_{F_{tract}} - D_a(v) - \mu_{CRR}(v)\cdot W_A\cdot\cos\phi - W_A\cdot\sin\phi \tag{1}$$

Here, $v=v_x$ is the instantaneous groundspeed (GS) in longitudinal direction and $a=a_x$ stands for the instantaneous translational acceleration. The symbol W_A is the airplane gravitational weight and g is the local terrestrial gravitational acceleration. Additive traction forces from NG and MG tires are designated as F_{tract}, aerodynamic drag with in-line wind component is D_a, speed-dependent CRR is μ_{CRR}, and the local TWY slope (grade) is ϕ (small angle in radians). For small grades $\cos\phi\approx 1, \sin\phi\approx\phi$. The aircraft's effective inertial mass $M_{eff}=\kappa\cdot M_A$ (inertial mass M_A) accounts for the added inertia of rotary components (wheels/tires, discs, rotors, axles, shafts, gears, transmissions, etc.)

$$\kappa = 1+\frac{1}{M_A}\sum_{j=1}^{n}\frac{i_j^2\cdot I_j}{r_j^2} \tag{2}$$

Here, I (kg m^2) stands for the mass moment of inertia, while non-dimensional factor i is the discrete gear-ratio and r is the effective radius of the rotating component. Using dedicated traction e-motor drives, the rotational inertia factor κ was estimated to contribute additional 1% to the

inertial mass (κ=1.01). The inertia of rotary components can often be neglected for contemporary large airplanes (Daidzic 2017). Maximum TWY and RWY longitudinal slopes are specified in ICAO and national airport/aerodrome design criteria (ICAO 2006, CAA 2014, FAA 2014) and are typically no steeper than 1.5% for aircraft approach categories C, D, and E. The maximum longitudinal grade change is 3% (FAA 2014). The transition between the longitudinal slopes must be gentle curved surface, i.e., slope rate change of no more than 1% variation in 30 m for aircraft approach categories C, D, and E (CAA 2014, FAA 2014). Transverse slopes are 1.5% for the same aircraft approach categories. Maximum sustained TWY/RWY slopes used here are 2% (about 1.15^o) to provide additional safety and performance factorization.

Internal resistances that come from various static and friction components in axles, shafts, bearings, brake rotors, etc., are not included in Eq. (1). Such internal resistances can be included into power transfer efficiency in combination with a motor-drive efficiency. Although the actual terrestrial gravitational acceleration changes slightly with latitude, and sometimes locally due to gravitational anomalies, we use the nominal standard (mid-latitude) value of 9.80665 m/s^2 (32.174 ft/s^2 or 19.05 kt/s) in all our computations. Lift force and partial unloading of tires generated at typical taxi speeds is neglected. The additional resistance coming from taxi turns was also neglected. The tractive propulsion system will have the reserve power to negotiate higher local grades and tight turns at low speeds if necessary. The total resistance R_{tract} for accelerated rolling with grade and aero-drag yields

$$R_{tract} = M_A\, g \cdot \left[\kappa \frac{a}{g} + \frac{D_a(v)}{W_A} + \mu_{CRR}(v) + \bar{\phi} \right] = \bar{\mu}_{req}\, M_A\, g \tag{3}$$

2.2 Electric traction

In several proposed green-taxi taxiing designs, the tractive force is supplied by separate NG and/or MG e-motors. For e-taxi purposes, the motor torque τ_m is delivered to tractive wheels τ_{wheel} via simple fixed transmissions. The dynamic (effective) radius of a tire (NG or MG as applicable) is designated as r_d. Driveshaft/powertrain tractive torque τ_{wheel} acts on the NG and/or MG wheel/tire assemblies. The relationship between the tractive force and the e-motor torque with the overall driveline efficiency η_t is

$$F_{tract} = \frac{\tau_{wheel}}{r_d} = \frac{\tau_m(N_m) \cdot i_{gbx} \cdot \eta_t}{r_d} \le F_{tract,max} \qquad i = \frac{N_{in}}{N_{out}} \tag{4}$$

The maximum (peak) tractive force on the tire on smooth hard surface (asphalt, concrete) depends on the vertical/normal load with the maximum CTF for various surface conditions, and for aircraft tires yields

$$F_{tract,max} = F_V \cdot \mu_{tract,max} \qquad \mu_{tract,max} = \left\{ \begin{matrix} 0.6-0.8 & \text{dry} \\ 0.4-0.6 & \text{wet} \\ 0.05-0.15 & \text{ice} \end{matrix} \right\}$$

Electric motors used in automotive traction applications, such as the Brushless DC motor (BLDC), Switched Reluctance Motor (SRM), AC-induction (AC asynchronous), etc., typically exhibit an ideal (hyperbolic) power-torque characteristic as shown in Fig. 2. The effective specific

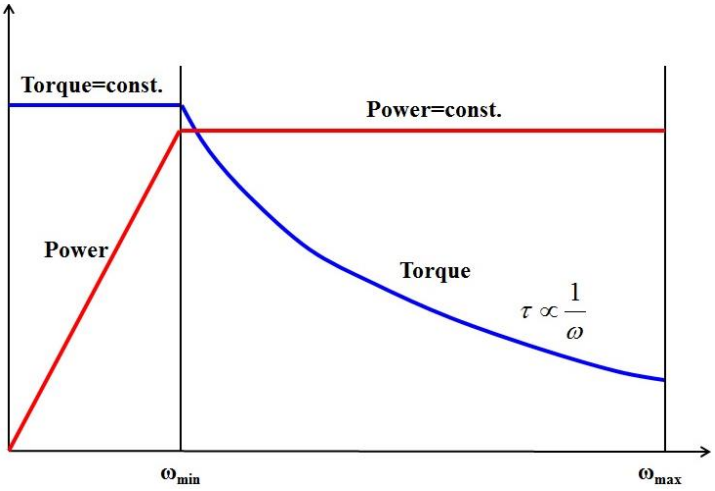

Fig. 2 An ideal hyperbolic torque-power characteristic of a typical traction electric motor. Not to scale

powers of AC 3ϕ tractive e-motors are 0.3 to 3 kW/kg depending on the cooling techniques and other factors (Miller 2004, Larminie and Lowry 2012). Many of e-motors can be overloaded for a short period, which is beneficial for taxi traction applications. However, for practical e-taxi applications, the overall motor specific-power of at least 5 kW/kg would be needed. Characteristics of electric machinery and motors in general and traction e-motors used in hybrid and electric road vehicles in particular is described by Gottlieb (1994), Fitzgerald *et al.* (2003), Miller (2004), Ehsani *et al.* (2010), and Larminie and Lowry (2012).

The effective tire radius is constant during taxiing and the gearbox (GBX) gear-ratio i_{gbx} is fixed (similar to final-drive in road vehicles). It is customary to express wheel or drive angular speeds in revolutions-per-minute (RPM). Tractive wheel angular speed and the airplane translational speeds are directly dependent on the instantaneous electric motor (BLDC, SRM, induction-type, etc.) rotational speeds

$$v = \omega_w \cdot r_d = \frac{2\pi}{60} \cdot N_w \cdot r_d = \frac{2\pi}{60} \cdot \frac{N_m}{i_{gbx}} \cdot r_d$$

For example, with a dynamic tire radius of 0.55 m, instantaneous e-motor rotational speed of 2,000 RPM, GBX ratio of 6.716:1, the wheel angular speed N_w is about 268 RPM and the airplane taxi speed is 30 knots (50.7 ft/s, 15.44 m/s, or 55.60 km/h). The RPM of modern aircraft electric motors is easily controlled using DC-Link (rectifiers) with the solid-state inverters, such as, IGBTs, MOSFETs, and Thyristors (Freitas and Daidzic 2017). An illustration of various speed-dependent tractive resistances and the electric motor tractive effort is shown in Fig. 3. Resistance due to turns is not included. The maximum speeds are obtained at the condition for which actual net driving force equals total net resistance F_{tract}=R_{tract}. Similar to railway operations and required locomotive net drawbar forces (Morlok 1978, Hay 1982), we can define an overall airplane taxi dispatch tractive (adhesion) coefficient

$$\overline{\mu}_{tract} = \frac{F_{tract}}{M_A g} \tag{5}$$

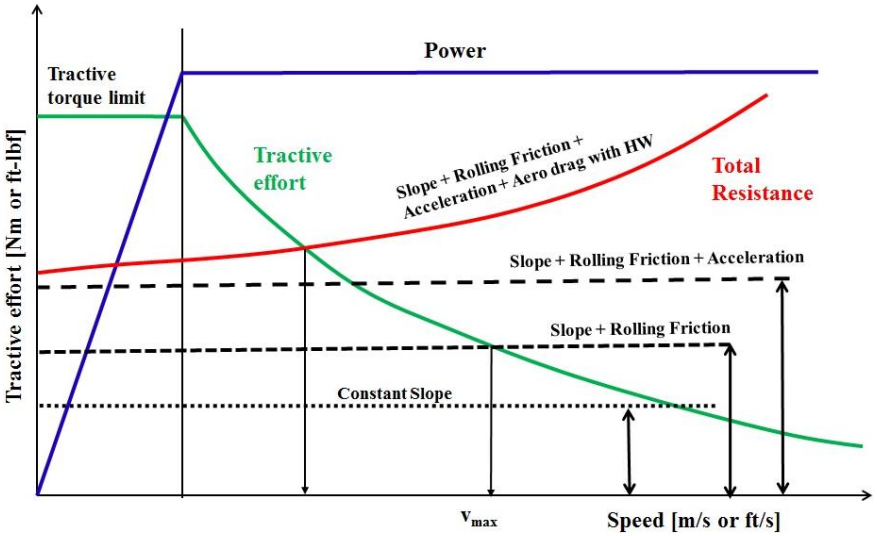

Fig. 3 An illustration of the total delivered tractive effort versus individual and combined resistances. Not to scale

2.3 Tire tractive capabilities and rolling resistances

For modern high-pressure aviation tires, the CRR increases slightly linearly with speed (for not too high speeds). We modified the linear relationship by Ehsani *et al.* (2010) for modern properly inflated high-pressure airplane tires (e.g., 170 psi NG and 200 psi MG for B767-300ER) with taxi speed in knots

$$\mu_{CRR}(v) = \mu_0\left(1+\frac{v}{v_0}\right) \qquad \mu_0 = f(p_{tire}) = 0.01 \quad v_0 = 80 \text{ kts} \qquad v \le 50 \text{ kts} \tag{6}$$

A typical value of the free-rolling CRR for high-pressure T-category airplane tires on smooth dry asphalt/concrete TWYs would be similar to truck tires with a CRR range 0.006 to 0.015 (Dixon 1996, Jazar 2008, Wong 2008, Ehsani *et al.* 2010). Tire's rolling resistance is about two orders-of-magnitude smaller than tractive/breaking efforts. The rolling friction also depends on tire operating pressures, construction, and other factors (Clark 1971, Wong 2008). Peak CTF values for wet asphalt are typically 20-40% lower than for dry. Maximum adhesive sliding/slipping (100%) CTFs for dry or wet asphalt pavements are 15-20% lower than respective peak values (Wong 2008). Peak CTF occurs typically around 15-20% slip. CTF peak and sliding CTF for dry and wet concrete pavement for several production truck tires are given in Wong (2008). Rolling resistance of modern tires is two-orders of magnitude lower than tractive or braking adhesion (grip). Yager (1990) provides useful experimental data on aircraft tire adhesion (grip) properties, including braking and cornering on dry and wet runways of older. While bias-ply tires have become almost extinct in passenger road vehicles (Braess and Seifert 2005) they are still quite common in aircraft tire applications. More details on tire construction, speed-dependent tire rolling resistance, and braking, tractive, and cornering properties can be found in Clark (1971), Gillespie (1992), Dixon (1996), Milliken and Milliken (2004), Braess and Seifert (2005), Jazar (2008), and Wong (2008).

2.4 Aerodynamic drag and wind resistances

The instantaneous aerodynamic drag for a typical T-category airplane in takeoff configuration while rolling in-ground-effect (IGE), with HW or tailwind (TW), is

$$D_a = G \cdot (v + v_w)^2 \qquad G = \frac{\rho_{SL} \cdot \sigma}{2} \cdot S_{ref} \cdot C_{D,takeoff} \qquad v_w \lesseqgtr 0 \tag{7}$$

The coefficient-of-drag for an airplane in takeoff configuration rolling IGE on a hard smooth surface is the sum of zero-lift drag and the drag-due-to-lift and can be expressed as

$$C_D = \left(C_{D,0} + \Delta C_{D,flap} + \Delta C_{D,gear}\right) + \beta \cdot K \cdot C_L^2 \tag{8}$$

The zero-lift drag (parasitic, interference, etc.) coefficient $C_{D,0}$ is typically in the range of 0.015-0.020 for fast modern swept-wing T-category airplanes in clean configurations (Nicolai and Carichner 2010, Raymer 1999) and can be approximately estimated as

$$C_{D,0} = C_{fe} \frac{S_{wet}}{S_{ref}} \qquad C_{fe} \cong 0.0025 - 0.0030 \qquad \frac{S_{wet}}{S_{ref}} \cong 4 - 7$$

We calculated the "wet" (exposed) surface area of each airplane model by numerical integration of known shapes and dimensions. The coefficient of skin-friction for laminar and/or turbulent boundary layer as appropriate was applied to the ratio of wet and wing reference area using methodologies described in Anderson (1999), Raymer (1999), McCormick (1995), and Nicolai and Carichner (2010). A small correction factor (about 25%) is typically added to the skin-friction factor C_f to account for small pressure (or form) drag due to small separation wakes, interference, and excrescence (protuberance) drag which is then designated as equivalent skin-friction factor C_{fe}.

The values of added parasitic drag due to extended flap and landing gear assembly are difficult to estimate accurately. Mostly such drag data come from wind-tunnel experiments and flight-test trials. Nicolai and Carichner (2010) suggest the values between 0.014 and 0.028 for the landing gear extended parasitic drag increment depending on the trailing edge flap deflection angle for some common T-category airplanes (e.g., for B747 in takeoff configuration it is about 0.025). Similar values are also suggested by Mair and Birdsall (1992). More detailed treatment of undercarriage drag can be found in Mair and Birdsall (1992) and Filippone (2012). Hence we used the expression suggested by Mair and Birdsall (1992) and Anderson (1999) which was also successfully used in Daidzic and Shrestha (2008) for landing roll calculations

$$\Delta C_{D,gear} = \left(\frac{W_A}{S_{ref}}\right) \cdot k_{gear} \cdot M^{-0.215}$$

The coefficient k_{gear} was chosen for the takeoff configuration (Mair and Birdsall 1992). The change of parasitic drag due to flap extension naturally depends on the amount of high-lift devices deployment. Typically for takeoff configuration (leading-edge high-lift devices fully deployed and trailing-edge high-lift devices partially extended) and existing production T-category airplanes we can assume this increment to be around 0.015 (Mair and Birdsall 1992). According to Nicolai and Carichner (2010) and Roskam and Lan (1997), the IGE influence factor β (drag-due-to-lift reduction due to modulated vortex dynamics affected by proximity of hard surface) can be estimated with

$$\beta = 1 - \frac{1 - 1.32 \cdot (h/b)}{1.05 + 7.4 \cdot (h/b)} \qquad 0.033 \le \frac{h}{b} \le 0.25 \qquad \frac{d\beta}{d(h/b)} > 0 \tag{9}$$

Typically for T-category airplanes considered here with given dihedral and washout in the main wings, the ratio (h/b) of the average height above ground h and wingspan b is in the range of 0.07-0.09 with the accompanied β in the range of 0.42-0.49. The coefficient of drag-due-to-lift K is typically in the range of 0.060 to 0.090 and accounts for lift-dependent parasitic drag k_1 and vortex/induced drag k_3 (wave drag component due-to-lift k_2 is non-existent at low Mach). For T-category airplanes in takeoff configuration with the Aspect Ratio (AR) and Oswald efficiency factor e, we can write (Anderson 1999)

$$K = k_1 + k_3 = k_1 + \frac{1}{\pi \cdot AR \cdot e} \qquad AR = \frac{b^2}{S}$$

Oswald or span-efficiency factor e depends on the wing planform and wing configuration (with quarter-chord sweep angle, Λ) and was estimated using methodology from Raymer (1999) and Nicolai and Carichner (2010). More or less detailed analytical treatment and various working relationships describing vortex drag and IGE drag reductions are given in Anderson (1991, 1999), Asselin (1997), McCormick (1995), Mair and Birdsall (1992), Filippone (2012), Raymer (1999), and Vinh (1993). The average coefficient of lift during taxiing is calculated from the finite-wing lift-curve slope and absolute incident AOA for rolling airplane IGE (Asselin 1997, McCormick 1995, Nicolai and Carichner 2010)

$$C_L = \left(\frac{dC_L}{d\alpha}\right)_0 \cdot \alpha_{IGE} \qquad \left(\frac{dC_L}{d\alpha}\right)_0 = C_{L,\alpha} = \frac{2\pi \cdot AR}{2 + \left\{4 + AR^2 \cdot \left[\left(1 - M^2\right) + tan^2 \Lambda\right]\right\}^{1/2}} < 2\pi$$

Quite generally, drag-due-to-lift represents small contribution at slow taxi speeds IGE and more detailed treatment of it is not warranted in this study.

2.5 Taxi fuel consumption

To estimate fuel consumption (FC) for standard taxiing cycle at the Maximum Ramp or design Taxi Weight (MRW), the jet engine(s) propulsive thrust is set equal to the taxiing resistances. In this analysis we only account for the fuel used for taxiing jet propulsion. Jet engine power off-takes (Giannakakis *et al.* 2011, Scholz *et al.* 2013) for various aircraft non-propulsive systems (Moir and Seabridge 2008, 2013, Wild 2008) are not considered as they may vary wildly and do not contribute to propulsion. As Nicolai and Carichner (2010) state, about 2.5% to 3% of the design maximum fuel weight is typically planned for the taxi fuel (takeoff and landing). Using the Thrust Specific Fuel Consumption (TSFC) and the thrust required in each segment, the instantaneous fuel flow, by neglecting power off-takes, is

$$\dot{m}_f = TSFC(v) \cdot T_{engines} = TSFC(v) \cdot R_{tract} \tag{10}$$

An expression for TSFC as a function of forward Mach number M and the temperature ratio θ for the generic high-bypass turbofan at low speeds is used (Daidzic 2016)

$$TSFC(\theta, M) = TSFC_0 \cdot \sqrt{\theta} \cdot (1 + M)^{0.8} \approx TSFC_0 \cdot \sqrt{\theta} \cdot (1 + 0.8 \cdot M) \qquad M << 1$$

This is an approximate semi-empirical relationship based on some historical engine data. $TSFC_0$ are values of TSFC at Sea-Level International Standard Atmosphere (SL ISA) and zero speed/Mach. For modern High Bypass-Ratio (HBPR) and Ultra-High BPR (UHBPR) turbofans this value is between 0.30 and 0.40 (lbm/hr) fuel per lbf thrust, which is equivalent to 30.59 to 40.78 g/N hr (lbm/lbf hr = 101.955 g/N hr = 28.321 mg/N s = 28.321 g/kN s). The fact is that $TSFC_0$ values are lower for UHBPR than for HBPR turbofans. The exact values of TSFC are extremely difficult to obtain from engine manufacturers. It was estimated here from cruise flight and other available data. At typical cruising altitudes (FL310 to FL430) and average cruise Mach numbers (0.78 to 0.85), TSFC has values between 0.55 to 0.65 lbm/lbf hr. Some of the TSFC values for various jet engines were also deduced from data given in Mattingly (2005), Hünecke (2000), and Treager (1995). An alternate way to estimate taxi movement only fuel flow and associated TSFC is to calculate the required thrust at a given speed for jet fuel used with associated engine thermal and propulsive efficiencies

$$\dot{m}_f = \frac{T_{engines} \cdot v}{\eta_{th} \cdot \eta_{pr} \cdot h_{LHV}} = \frac{P_{tract}}{\eta_{th} \cdot \eta_{pr} \cdot h_{LHV}} \tag{11}$$

Thrust of contemporary turbofan engines at slow speeds accounting for constant wind (speeds are true airspeeds or TAS) can be expressed as (Daidzic 2016)

$$T_{engines}(\sigma, v) \approx n_e \cdot N_1 \cdot T_{SL,ISA}^{static} \cdot \sigma^m \cdot \left[1 + c_1 \cdot (v + \bar{v}_w)\right] \qquad c_1 < 0$$

Here, density ratio σ exponent m is 0.7 at low altitudes, n_e is the number of operating engines, and N_1 is throttle (thrust) setting parameter. The speed coefficient c_1 in an engine momentum-drag term depends on many factors and is numerically different for every jet engine under consideration (Daidzic 2016). The enthalpy (LHV) of typical commercial HC jet fuels is in the 42-44 MJ/kg range. The stoichiometric fuel/air ratio for modern HC JP fuels is about 0.0670-0.0680 with the average HC fuel mass density in the range of 750 to 850 kg/m^3 (Treager 1995, Asselin 1999, Mattingly 2005). The total FC during taxiing is now calculated by integrating instantaneous fuel flow over taxi duration in all segments

$$\Delta m_f = \int_0^t \dot{m}_f(t) \cdot dt \tag{12}$$

The purpose of taxi-FC computations is to estimate the amount of fuel spent during standard taxi cycle. Accordingly, the estimates of air pollution can be conducted or the fuel saved computed if the main propulsive jet engines are not used. The actual taxi distances and durations can vary significantly in line-operations. Fuel and TSFC computed does not account for the fuel needed for power off-takes for other non-propulsive systems (electrical, pneumatic, hydraulic, etc.)

2.6 Taxi cycle

To test the requirements of the airplane traction taxi concept we devised a “standard” taxi cycle (schedule) of effective straight distance with three intermediate stops and the fourth final stop (before jet-engines start). The “standard” taxi configuration is illustrated in Fig. 4. Basic characteristics of standard taxi cycles or schedules are summarized in Table 1. A combination of various surface grades, HWs, coasting speeds, and accelerations were used to test probable worst case conditions.

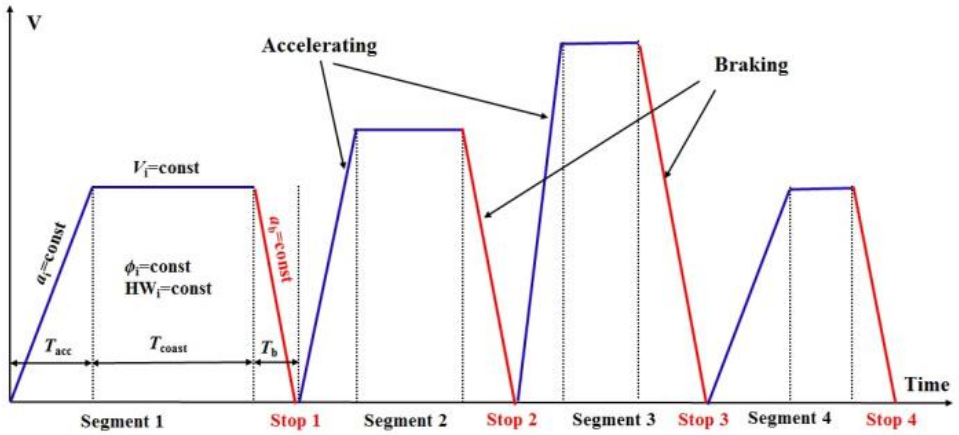

Fig. 4 A proposed airplane taxiing cycle for T-category airplanes at large airports for the evaluation of tractive taxi requirements. Not to scale

Table 1 Proposed airplane taxi cycles at large airports in SL ISA conditions

Segment	S_1	S_2	S_3	S_4	Total or Average
t_{tract} (sec)	150	90	90	120	450*
v (kt) (m/s)	20 (10.3)	30 (15.45)	35 (18.025)	25 (12.875)	23.51/12.11
s (ft)	4,728.89	4,053.33	4,285.56	4,802.78	17,870.56*
$\bar{a}$ (kt/s) (m/s^2)	+1.0 (0.515)	+1.5 (0.773)	+1.0 (0.515)	+2.0 (1.03)	NA
HW (kt) (m/s)	10 (5.15)	20 (10.3)	20 (10.3)	30 (15.45)	NA
$\bar{\phi}$ (%) (deg.)	0. (0.)	1.0 (0.573)	1.0 (0.573)	2.0 (1.146)	NA
$\bar{a}_b$ (kt/s) (m/s^2)	-4.0 (-2.06)	-4.0 (-2.06)	-4.0 (-2.06)	-4.0 (-2.06)	NA

*Note: Tractive time and distance only. Total braking time adds 27.50 seconds and 665.0 ft to tractive time and distance

This information is required for the design of tractive units. Total taxiing distances, stored energy consumption, as well as the average, coasting and the peak instantaneous powers were computed in each segment. Average sustained accelerations from standstill until coasting constant speeds are achieved were used. The exact order of segments is unimportant. Unlike jet-engines idling and still using fuel while stopped and waiting during taxi operations, electric tractive systems are not used unless needed. Some of the proposed e-taxi methods envision RB, but it is not clear how that would be accomplished. Distance covered in each discrete taxi segment and the total airplane taxi distance can be determined from

$$L = \sum_{i=1}^{4} s_i = \sum_{i=1}^{4} \left(\int_{t_{i-1}}^{t_i} v_i \cdot dt \right) \qquad v_i(t) = \begin{Bmatrix} \bar{a}_i t & 0 \le t < t_{acc} \\ \bar{v}_i & t_{acc} \le t \le t_b \\ -\bar{a}_b t & t > t_b \end{Bmatrix} \tag{13}$$

Distances covered during constant acceleration phase at varying acceleration durations, during coasting at constant speed, and finally braking deceleration are accounted for. Integration for each individual segment (from standstill to the onset of braking) and separately for braking alone yields

$$s_i = \bar{v}_i \cdot t_i - \frac{\bar{v}_i^2}{2 \cdot \bar{a}_i} \qquad s_{bi} = \frac{\bar{v}_i^2}{2 \cdot \bar{a}_b} \tag{14}$$

Traction work/energy used during each segment can be calculated from

$$A_{tot} = \sum_{i=1}^{4} A_i = \sum_{i=1}^{4} \left(\int_{s_{i-1}}^{s_i} F_i \cdot ds \right) = \sum_{i=1}^{4} \left(\int_{t_{i-1}}^{t_i} F_i \cdot v_i(t) \cdot dt \right) \tag{15}$$

The net force and accelerations (zero during constant-speed coasting) in each segment (starting from standstill) is calculated by substituting Eq. (1) into Eq. (15). The total tractive work required for each accelerate-coast segment with constant wind (HW or TW) was derived here

$$\begin{aligned} A_i = {} & \underbrace{\frac{M_A \cdot \kappa \cdot \bar{v}_i^2}{2}}_{\text{Inertia}} + \underbrace{M_A\, g \bar{\phi}_i s_i}_{\text{Grade}} + \underbrace{M_A\, g\, \mu_0\, s_i + M_A\, g\, \mu_0 \frac{\bar{v}_i}{v_0} \left(s_i - \frac{1}{3} \frac{\bar{v}_i^2}{2\bar{a}_i} \right)}_{\text{Rolling friction}} + \\ & \underbrace{+ G \cdot \frac{\bar{v}_i^2}{2\bar{a}_i} \left(\frac{\bar{v}_i^2}{2} + \frac{4}{3} \bar{v}_i \bar{v}_w + \bar{v}_w^2 \right) + G \cdot (\bar{v}_i + \bar{v}_w)^2 \left(s_i - \frac{\bar{v}_i^2}{2\bar{a}_i} \right)}_{\text{Aero-Drag with Wind}} \end{aligned} \tag{16}$$

Accordingly, Eq. (16) is just a simple manifestation of the conservation of energy. No crosswind (XW) or turning/steering dynamics was accounted for. Change of mass/weight during taxi maneuver is neglected (less than 0.2% weight change). MRW was used for initial design requirements. The average power used in each segment is

$$\bar{P}_i = \frac{A_i}{t_i} \tag{17}$$

The rated tractive power to coast at a constant speed with steady wind and surface grade is

$$P_i = \left\{ M_A\, g \cdot \left[\mu_{CRR}(\bar{v}_i) + \bar{\phi} \right] + G \cdot (\bar{v}_i + \bar{v}_w)^2 \right\} \cdot \bar{v}_i \tag{18}$$

The maximum (peak) net traction power at designed (required acceleration at design speed) is

$$P_{max} = T_d \cdot v_d = \left\{ M_A \cdot \kappa \cdot a_d + D_{a,d} + M_A\, g \cdot \left[\mu_{CRR}(\bar{v}_d) + \bar{\phi}_d \right] \right\} \cdot v_d \tag{19}$$

Total tractive resistances can be modeled as a 2nd-order polynomial using Eq. (3)

$$\frac{R_{tract}}{M_A\, g} = \bar{\mu}_{tract} = A + B \cdot v + C \cdot v^2 \tag{20}$$

with

$$A = \kappa \frac{a}{g} + \mu_0 + \bar{\phi} \qquad B = \frac{\mu_0}{v_0} \qquad C = \frac{\rho_{SL} \cdot \sigma}{2} \cdot \frac{C_{D,tkoff}}{(W_A / S_{ref})} \qquad A >> B >> C$$

This resembles resistance equations for road vehicles and trains (Morlok 1978, Hay 1982). No internal resistances have been considered in Eq. (20).

Table 2 Basic features of production airplane models used in taxi computations

Airplane Model	E190	B737-800	B767-300 (ER)	A340-300	B747-8I	A380-800
MRW	115,000	174,000	413,000	612,000	990,000	1,274,000
(lb/kg)	52,154.2	78,911.6	187,301.6	277,551	448,979.6	577,777.8
S_{ref}	996	1,341.2	3,050	3,908	5,960	9,100
(ft^2/m^2)	92.53	124.6	283.36	363.07	553.72	845.44
b	94.3	112.6	156.1	197.8	224.6	261.7
(ft/m)	28.73	34.32	47.57	60.30	68.45	79.76
Engine	2x GE	2x CFM56-	2x PW	4x	4x	4x RR
model	CF3410E	7B24/26/27	4056/60/62	CFM56-5C	GEnx-2B67	Trent 900

Note: Small discrepancies in MRW values may exist for specific airplane models. For some airplane models there are several engine options

3. Results and discussion

Four full stops (three intermediate) are assumed during "standard" taxiing cycle for takeoff. Landing weights are significantly lower and so are tractive forces, energy, and power requirements. Four representative taxi segments were considered with various associated TWY (occasionally RWY) slopes, HW, sustained accelerations, and coasting speeds. Braking acceleration was assumed not abrupt at about 0.2 g and is constant for all four stops. Basic characteristics of standard taxi cycles or schedules were already given in Table 1. The exact order of segments is irrelevant due to taxiing time, distance, and energy cumulative and commutative properties. In reality, large combination of taxi-in and -out distances and routes exists on large airports and principally depends on traffic load, atmospheric wind, ATC restrictions, etc. ATC and congestion taxiing delays were not considered. Basic design characteristics for different airplanes used in taxi computations are summarized in Table 2. About 40 different geometric, performance, and aerodynamic parameters were used for each airplane/powerplant combination. Since many values had to be estimated using accepted methodologies or reverse-engineer from known conditions, we do not make any claims or statements that calculated values faithfully represent specific airplane and powerplant models. Limited numerical sensitivity and uncertainty analysis has been performed by varying some of the operationally-sensitive variables (CRR, C_D in takeoff configuration, etc.) and it was found that their effects are rather small. Hence, we believe that estimated values of driving resistances are credible and accurate to within 1-2%. However, conducting experiments with real airplanes on realistic taxi routes should not be that difficult.

Airbus A320-200 is very similar in size to B737-800 so they practically share results obtained here. Some variations may exist in exact MRW for specific production airplane models. The jet engine effective TSFC will depend on the particular engine model and also depend on the existing power off-takes. We used best estimates of TSFC to obtain approximate fuel amounts for standard taxi operations. It is assumed that all tires are inflated to their proper values. The exact CRR may vary slightly for different tire models used. Takeoff configuration may vary slightly from model to model and for various takeoff conditions. Aircraft tire and gear loading data was obtained from manufacturer (Boeing 2005, 2012, 2013) when available or from consulting various sources and using best estimates. Aircraft Classification Numbers (ACN) and Pavement Classification Numbers (PCN) numbers were calculated based on the exact loading and MAC setting (CAA 2014, FAA 2014, Swatton 2008).

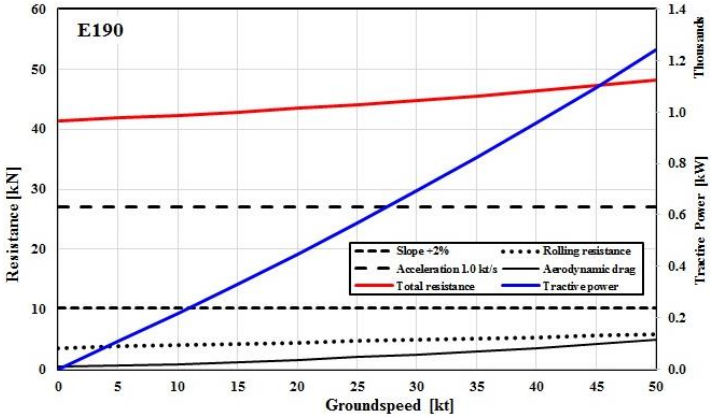

Fig. 5 Calculated individual and combined taxi resistances and tractive power for E190 at given sustained acceleration of 1 kt/s, 1% upslope, and 20 kt HW

Table 3 Summary taxi performance calculations for E190 using proposed taxi cycle

E190	S_1	S_2	S_3	S_4	Total or Average
F_{coast} (kN)	7.29	14.63	15.47	19.94	NA
$F_{acc,m}$ (kN)	34.41	55.31	42.59	74.19	NA
E (MJ)	13.187	24.058	28.022	33.422	98.689
P_{av} (kW)	87.98	267.52	311.60	278.73	NA
P_{max} (kW)	354.51	854.81	767.92	955.46	NA
P_{coast} (kW)	75.08	226.08	278.92	256.87	NA
FC (kg)	12.07	14.74	14.92	24.37	66.10

Note: NA-Not Applicable

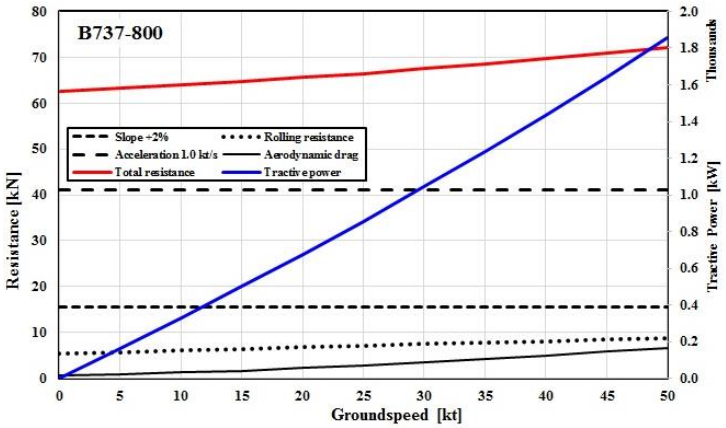

Fig. 6 Calculated individual and combined taxi resistances and tractive power for B737-800 at given sustained acceleration, upslope, and HW

Calculated individual and combined total resistance forces and tractive power for Embraer E190 regional jet taxiing on a constant 2% upslope with sustained 1 kt/s (about 0.5 m/s^2)

Table 4 Summary taxi performance calculations for B737-800 using proposed taxi cycle

B737-800	S_1	S_2	S_3	S_4	Total or Average
F_{coast} (kN)	10.90	21.79	22.99	29.77	NA
$F_{acc,m}$ (kN)	51.94	83.35	64.03	111.84	NA
E (MJ)	19.781	36.000	41.909	49.978	147.667
P_{av} (kW)	131.98	400.31	466.01	416.80	NA
P_{max} (kW)	535.14	1,288.12	1,154.51	1,440.36	NA
P_{coast} (kW)	112.34	336.83	414.61	383.38	NA
FC (kg)	18.38	22.38	22.63	36.99	100.38

Note: NA-Not Applicable

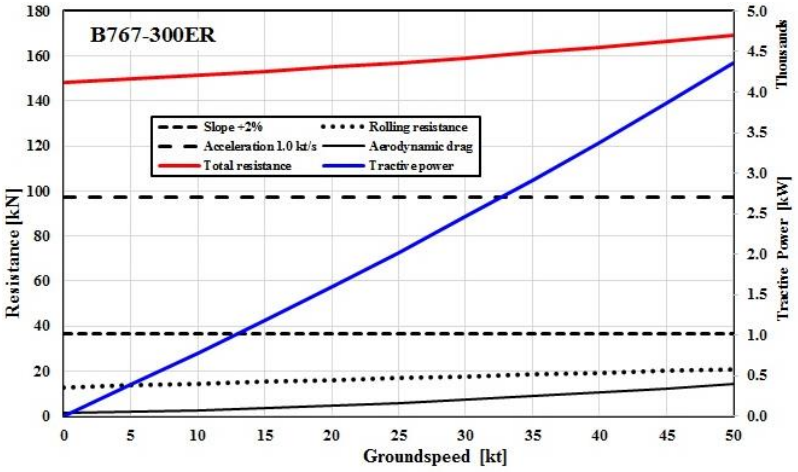

Fig. 7 Calculated individual and combined taxi resistances and tractive power for B767-300ER at given sustained acceleration, constant upslope, and HW

Table 5 Summary taxi performance calculations for B767-300ER using proposed taxi cycle

B767-300ER	S_1	S_2	S_3	S_4	Total or Average
F_{coast} (kN)	25.55	50.81	53.46	69.53	NA
$F_{acc,m}$ (kN)	122.94	196.90	150.86	264.33	NA
E (MJ)	46.484	84.354	98.137	117.011	345.986
P_{av} (kW)	310.14	937.99	1,091.26	975.85	NA
P_{max} (kW)	1,266.75	3,043.14	2,720.11	3,404.38	NA
P_{coast} (kW)	263.21	785.20	963.93	895.55	NA
FC (kg)	43.82	53.20	53.73	87.88	238.64

Note: NA-Not Applicable

translational acceleration, and into 20 knots steady HW at various groundspeed (GS) are shown in Fig. 5. Summary of net resistances and net required traction forces and power for an E190 is given in Table 3. Note that FC values (last row) do not account for power off-takes needs.

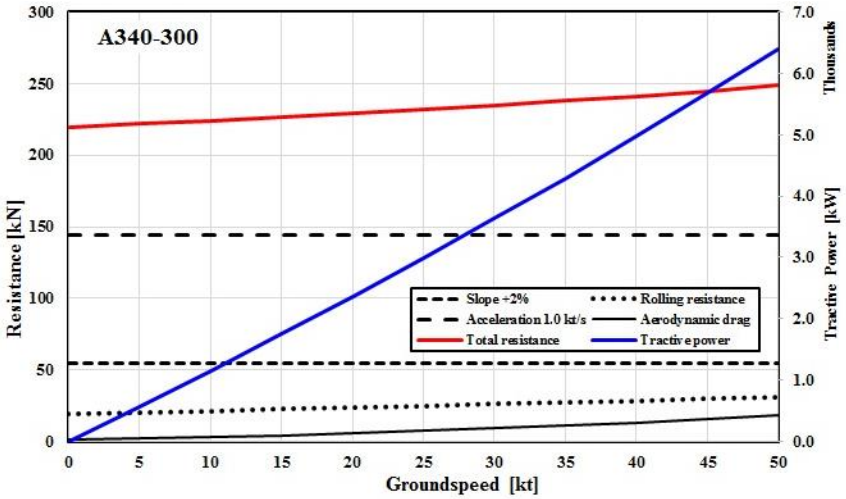

Fig. 8 Calculated individual and combined taxi resistances and tractive power for A340-300 at given sustained acceleration, constant upslope, and HW

Table 6 Summary taxi performance calculations for A340-300 using proposed taxi cycle

A340-300	S_1	S_2	S_3	S_4	Total or Average
F_{coast} (kN)	37.40	74.02	77.69	101.51	NA
$F_{acc,m}$ (kN)	181.72	290.52	222.02	390.17	NA
E (MJ)	68.245	123.505	143.600	171.188	506.538
P_{av} (kW)	455.32	1,373.34	1,596.79	1,427.67	NA
P_{max} (kW)	1,872.43	4,489.94	4,003.23	5,025.07	NA
P_{coast} (kW)	385.36	1,144.03	1,400.85	1,307.39	NA
FC (kg)	62.43	75.58	76.25	124.78	339.03

Note: NA-Not Applicable

Graphical result for B737-800 (can also be used for A320-200) taxiing resistance characteristics and at the same conditions as for E190 previously is given in Fig. 6. Numerical values of resistances and tractive requirements are summarized in Table 4. The results for popular twin-engined long-range 180-minutes ETOPS B767-300ER (Extended Range) are given in Fig. 7 and Table 5 respectively. To no surprise the magnitude of forces, power and taxi fuel use increased with the airplane weight. The results for 4-engined long-range A340-300 heavy are given in Fig. 8 and Table 6 respectively. As expected the magnitude of forces, power, and taxi fuel use increased further with the airplane weight.

The results for 4-engined ultra long-range B747-8I with MRW of almost one million pounds are given in Fig. 9 and Table 7 respectively. As expected the magnitude of forces, power, and taxi fuel use increased further with the airplane weight. The results for 4-engined long-range A380-800 with MRW of almost 1.3 million lb (mass almost 578,000 kg) are given in Fig. 10 and Table 8 respectively. A380-800 is the biggest airplane in passenger commercial air-transportation service though not the biggest airplane in service today. The magnitude of tractive forces and power requirements as well as taxi fuel are truly extraordinary.

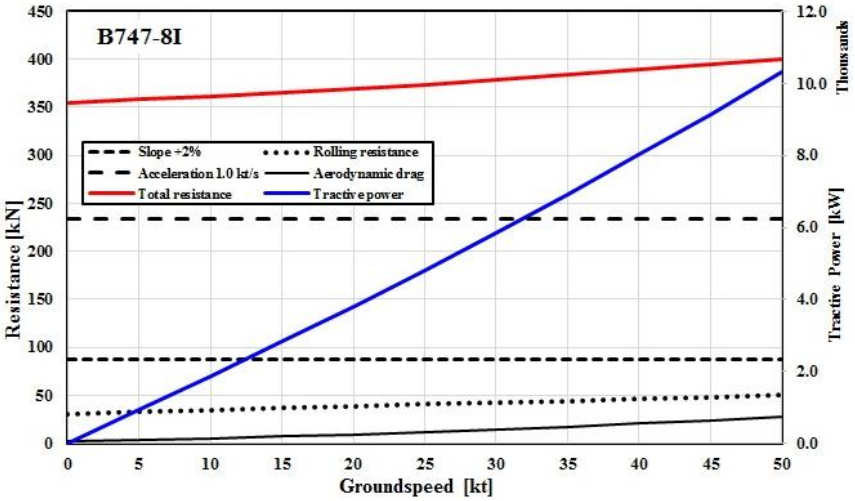

Fig. 9 Calculated individual and combined taxi resistances and tractive power for B747-8I at given sustained acceleration, constant upslope, and HW

Table 7 Summary taxi performance calculations for B747-8I using proposed taxi cycle

B747-8I	S_1	S_2	S_3	S_4	Total or Average
F_{coast} (kN)	60.15	118.78	124.51	163.04	NA
$F_{acc,m}$ (kN)	293.61	468.99	357.98	629.99	NA
E (MJ)	109.908	198.646	230.901	275.238	814.694
P_{av} (kW)	733.29	2,208.89	2,567.56	2,295.43	NA
P_{max} (kW)	3,025.36	7,248.23	6,454.76	8,113.76	NA
P_{coast} (kW)	619.80	1,835.72	2,245.03	2,099.86	NA
FC (kg)	100.53	121.54	122.55	200.60	545.22

Note: NA-Not Applicable

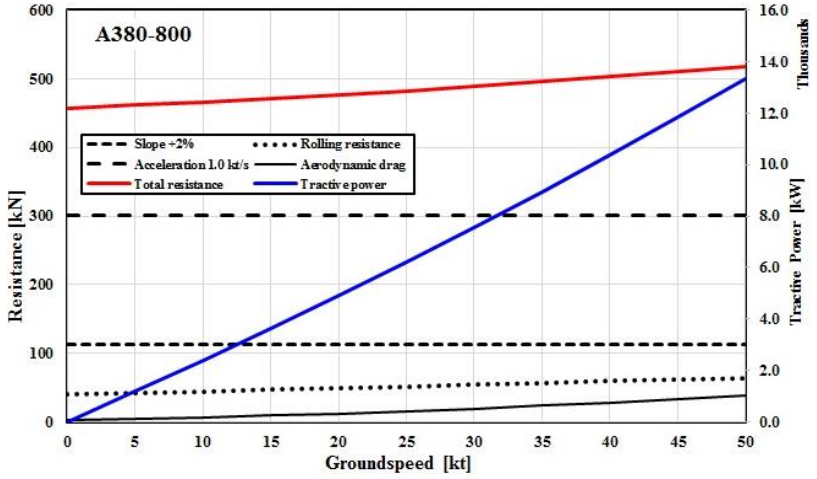

Fig. 10 Calculated individual and combined taxi resistances and tractive power for A380-800 at given sustained acceleration, constant upslope, and HW

Table 8 Summary taxi performance calculations for A380-800 using proposed taxi cycle

A380-800	S_1	S_2	S_3	S_4	Total or Average
F_{coast} (kN)	77.92	154.27	161.95	211.54	NA
$F_{acc,m}$ (kN)	378.36	604.95	462.40	812.43	NA
E (MJ)	142.156	257.314	299.193	356.677	1,055.340
P_{av} (kW)	948.44	2,861.26	3,326.95	2,974.61	NA
P_{max} (kW)	3,898.51	9,349.50	8,337.46	10,463.51	NA
P_{coast} (kW)	802.87	2,384.31	2,920.09	2,724.41	NA
FC (kg)	126.10	152.69	154.06	252.10	684.95

Note: NA-Not Applicable

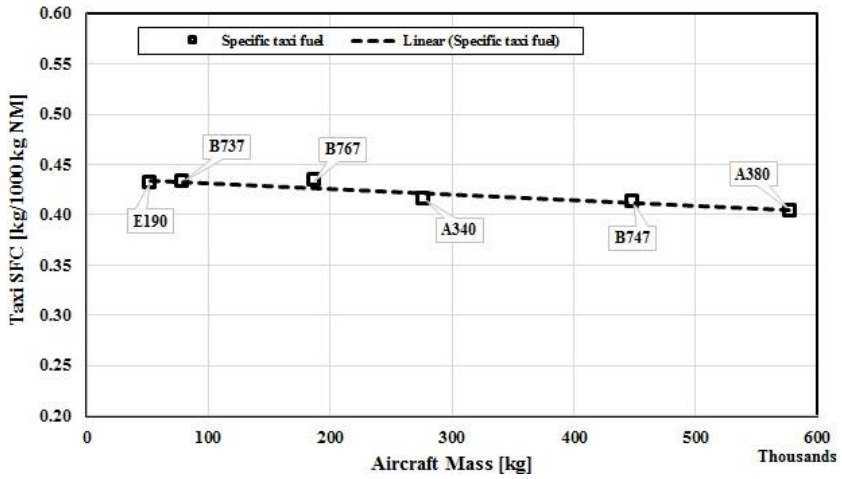

Fig. 11 Taxi specific fuel consumption (SFC) in kg of fuel per each 1,000 kg of airplane taxi mass and per one effective taxi NM (stops and systems power off-takes not accounted)

The results for each airplane and the linear trend-line of taxi fuel used for various aircraft scaled with their respective masses is shown in Fig. 11. Accordingly, any T-category airplane will use, on average, about 0.42 kg of fuel for each 1,000 kg of airplane taxi mass per NM (1.852 km) taxi distance. This simple rule holds reasonably well for all airplane models considered here. Since the total tractive distance is 5,445 m (2.94 NM), the total average taxi FC for proposed taxi cycle is about one kg of fuel per each 806 kg of airplane or about 1.24 kg of fuel for each 1,000 kg of airplane mass.

The net tractive forces increase perfectly linearly with the mass/weight defining an overall tractive coefficient which is airplane mass independent. This result is visually clear from Fig. 12. For coasting under given conditions, the operational net tractive coefficient is 0.035 (3.5%). For the worst case scenario where large accelerations are needed in conjunction with HW and 1% upslope, the operational taxi tractive coefficient required is around 0.14 (14%). Also shown is the tractive force requirement with the operational tractive coefficient of 0.1 for which the linear regression line shows almost perfect match. This is not surprising as the linear and quadratic speed-dependent terms are very small in Eq. (20). Quite generally, all tractive force versus mass regressions are almost perfectly linear since the coefficient *A* in Eq. (20) dominants. Calculated ground idle thrust from all installed jet engines (7% of maximum) is insufficient to meet tractive

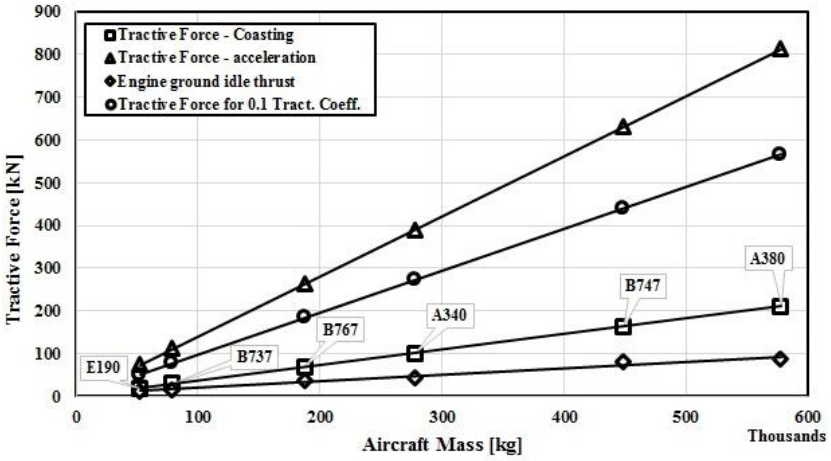

Fig. 12 Acceleration and coasting resistance for various airplane models in the 4th segment (S4) under defined conditions (Table 1)

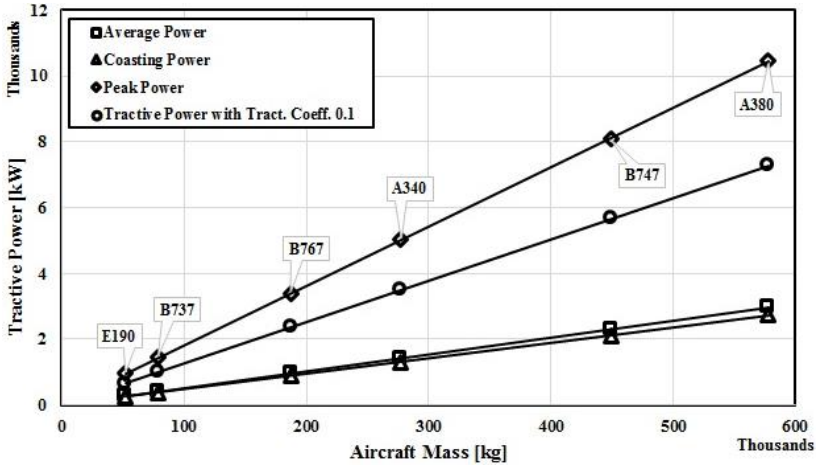

Fig. 13 Calculated individual and combined taxi resistances and tractive power for A380-800 at given sustained acceleration, constant upslope, and HW

needs in this segment. For example, taxi thrust at 7% (Teo *et al.* 2008) of the maximum rated installed thrust of two PW4060 engines produces about 38.3 kN at SL and is sufficient for B767-300ER to coast at almost 30 knots on a +1% grade with zero HW. Taxiing into 20 kt HW at the same +1% grade, the maximum speed achieved with the 7% SL taxi-thrust would be about 17 kt. For the taxi cycle proposed here, the 7% of max-thrust level would be sufficient only in the first segment (see Table 5) and is about half needed for coasting in the 4th segment. Boeing's ground towing data for B767 family (Boeing 2005) implies required drawbar force of 110 kN for a +2% grade, jet engines at zero-thrust, and a 20,000 kg total tug traction wheel load on a wet concrete with CTF of 0.57. While the acceleration and speed data were not explicitly provided by Boeing, we estimated average acceleration of a tow truck at about 0.3 m/s^2 (about 0.6 kt/s), which is reasonable. One should be careful not to confuse data for tow truck tires designed for traction with the airplane tires.

Average, coasting, and peak required net tractive power is shown in Fig. 13. Tractive power with the operational tractive coefficient of 0.1 (10%) is also shown. Unavoidable losses due to generation and transmission of electrical power and motor losses must be additionally accounted for. There is practically no difference between the average and coasting power in the fourth segment. For example, just to coast in the fourth segment an E190 will need 250-280 kW total, while an A380-800 will need almost 3,000 kW. Peak power is about four times higher. By relaxing the taxiing acceleration requirements, lower design powers are needed, but that again will be decided by certification agencies, manufacturers, and air-transportation industry.

The need for reduced air and noise pollution and reduction of taxiing fuel costs have resulted in development of green e-taxiing concepts. Trends toward MEA aircraft designs have facilitated such concepts which are based on embedding traction e-motors in NGs and/or MGs. Such concepts have been used in diesel-electric locomotives for over 60 years and in the case of electric-locomotives more than 100 years. For example, modern diesel-electric locomotives have (DC or AC) individual traction e-motors delivering about 1,000 HP (746 kW) per powered axle. Such motors with speed and traction control typically work at maximum 600 V and can pull currents in excess of 1,000 Amperes, requiring thick and heavy conductors.

The supply of electrical power for airplane traction motors comes from onboard APU(s). However, NG-traction alone may not suffice for larger T-category airplanes and on surfaces other than perfectly dry and level with high CTF. The problem with the MG traction-motors as that the wheel space is already occupied by friction brakes. Additionally, the APUs even in most modern MEAs are unlikely to deliver sufficient amount of traction power. Battery storage systems can be used to supplement APUs. However, battery systems are still very limited and deliver maximum specific power today in commercial for Li-Ion (LIB) batteries is in the range of 300-500 W/kg (Larminie and Lowry 2012). For example, to supplement APU's 250 kW for traction motors with another 500 kW, realistically about 1,000 kg (2,205 lb) in LIB batteries are needed. Future developments will certainly increase battery specific energies and power, but that may not be sufficient. Add to that the weight of the traction motors, simple transmissions, and all the wires and harnesses and the weight penalty may be excessive for FAR/CS 25 certified airplanes. Additionally, there is acute safety problem with LIB batteries in aerospace applications. Hence, it is not clear how the currently developed electric tractive technologies will succeed regarding the landing gear space constraints, harsh environment, and e-motor power limitations. Depending on the T-category airplane size, four to ten traction motors embedded in the NG and the MG wheels in the range 100 to 400 kW per unit (for 400 to 4,000 kW range) would be most probably needed for reliable independent and autonomous e-taxi airport ground movements. Especially large tractive forces and power are needed for required airplane taxi accelerations. Existing e-motor technology cannot reliably provide specific power and power densities required for large and very large T-category airplanes. Additionally, existing NG designs may not be able to sustain repeated bending forces caused by tractive forces. Regarding MG traction, the problem of high brake temperatures after landings (or rejected high-speed takeoffs) may obstruct the operation of tractive e-motors.

4. Conclusions

A taxiing cycle was proposed in order to understand taxiing performance requirements, tractive forces, and power needed for T-category airplanes. The cycle represents a reasonably adverse

combination of various expected taxiway positive grades, steady HWs, and required accelerations in the case of urgency to clear the taxiway or when crossing active runways. The standardized pattern/schedule involves taxi distance in excess of 3 NM with three intermediate and one final stop before main engines start. Taxi-in movement after landing reduces performance requirements of the tractive system. The total taxi-out movement lasts about 8 minutes and does not include delays with idling jet engines. Six different airplanes used in commercial air transportation from E190 regional jet to behemoth A380-800, were simulated during taxiing operations under equal conditions. Not unexpectedly, it was found that the total tractive force and power requirements increase linearly with the airplane's weight/mass. As anticipated the largest resistance comes from the inertial forces followed by grade and rolling resistances. Tractive propulsion and rolling resistances are very sensitive to tire/surface conditions. Aerodynamic drag together with headwind only plays important role at higher taxi speeds and strong headwinds. Internal resistances are not included in calculated required tractive forces. Even the most powerful existing airport tow trucks are unable to deliver required drawbar pull/push for heavier airplanes negotiating reasonably up-sloped taxiways, while heading into stiff headwind at low speeds. All current production airplane models are power-limited using APUs for e-taxi traction motors other than for level surfaces and coasting at very low speeds. Hybrid taxi solutions using additional dedicated traction batteries located in an aircraft would significantly increase inert mass/weight and add further design complications. Reliable independent taxiing can be achieved if the overall net operational tractive coefficient is 0.1 and higher.

References

Anderson, J.D. (1991), *Fundamentals of Aerodynamics*, 2nd Edition, McGraw-Hill, New York, U.S.A.

Anderson, J.D. (1999), *Aircraft Performance and Design*, McGraw-Hill, New York, U.S.A.

Asselin, M. (1997), *An Introduction to Aircraft Performance*, American Institute for Aeronautics and Astronautics (AIAA), Reston, U.S.A.

Boeing (2005), *767 Airplane Characteristics for Airport Planning (D6-58328)*, Boeing Commercial Airplanes Seattle, U.S.A.

Boeing (2012), *747-8 Airplane Characteristics for Airport Planning (D6-58326-3)*, Boeing Commercial Airplanes, Seattle, U.S.A.

Boeing (2013), *737 Airplane Characteristics for Airport Planning (D6-58325-6)*, Boeing Commercial Airplanes, Seattle, U.S.A.

Braess, H.H. and Seifert, U. (2005), *Handbook of Automotive Engineering*, Society of Automotive Engineers International (SAE), Warrensdale, U.S.A.

Civil Aviation Authority (UK CAA) (2014), *CAP 168: Licensing of Aerodromes*, 10th Edition, Civil Aviation Authority, West Sussex, U.K.

Clark, S.K. (1971), *Mechanics of Pneumatic Tires (NBS Monograph 122)*, National Bureau of Standards, Washington, U.S.A.

Daidzic, N.E. (2016), "Estimation of performance airspeeds for high-bypass turbofans equipped transport-category airplanes", *J. Aviat. Technol. Eng.*, **5**(2), 27-50.

Daidzic, N.E. (2017), "Modelling and computation of the maximum braking energy speed for transport category airplanes", *J. Aviat. Technol. Eng.*, **6**(2), 2-25.

Daidzic, N.E. and Shrestha, J. (2008), "Airplane landing performance on contaminated runways in adverse conditions", *J. Aircraft*, **45**(6), 2131-2144.

Dixon, J.C. (1996), *Tires, Suspension and Handling*, 2nd Edition, Society of Automotive Engineers International (SAE), Warrendale, Pennsylvania, U.S.A.

Ehsani, M., Gao, Y. and Emadi, A. (2010), *Modern Electric, Hybrid Electric and Fuel Cell Vehicles*, 2nd Edition, CRC Press, Florida, U.S.A.

Filippone, A. (2012), *Advanced Aircraft Flight Performance*, Cambridge University Press, Cambridge, U.K.

Fitzgerald, A.E., Kingsley, C. and Umans, S.D. (2003), *Electric Machinery*, 6th Edition, McGraw-Hill, New York, U.S.A.

Freitas, E.F.C. and Daidzic, N.E. (2017), "Design of DC-link VSCF AC electrical power system for embraer 190/195 aircraft", *J. Aviat. Technol. Eng.*, **7**(1), 19-44.

Giannakakis, P., Laskaridis, P. and Pilidis, P. (2011), "Effects of off-takes for aircraft secondary-power systems on jet engine efficiency", *J. Propul. Pow.*, **27**(5), 1024-1031.

Gillespie, T.D. (1992), *Fundamentals of Vehicle Dynamics*, Society of Automotive Engineers International (SAE), Warrendale, Pennsylvania, U.S.A.

Gottlieb, I.M. (1994), *Electric Motors and Control Techniques*, 2nd Edition, McGraw-Hill, New York, U.S.A.

Hay, W.W. (1982), *Railroad Engineering*, 2nd Edition, John Wiley & Sons, New York, U.S.A.

Heleno, T.A., Slama, J.G. and Bentes, F.M. (2014), "Analysis of airport noise through L_{Aeq} noise metrics", *J. Air Transp. Manage.*, **37**, 5-9.

Hershey, R.L. and Turner, L. (1974), "Taxiing noise of jet aircraft", *J. Acoust. Soc. Am.*, **56**(S1), S34-S35.

Hospodka, J. (2014), "Electric taxiing-taxibot system", *Mag. Aviat. Develop.*, **2**(10), 17.

Hughes, K., Nutaro, J. and Haissig, C.M. (2013), *Electric Taxi Auto-Guidance and Control System*, US Patent, US 8,620,493.

Hünecke, K. (2000), *Die Technik Des Modernen Verkehrsflugzeuges (2. Auflage)*, Motorbuchverlag, Stuttgart, Germany.

ICAO (2006), *Aerodrome Design Manual*, 3rd Edition, International Civil Aviation Organization, Montreal, Canada.

Ignaccolo, M. (2000), "Environmental capacity: Noise pollution at Catania-Fontanarossa international airport", *J. Air Transp. Manage.*, **6**(4), 191-199.

International Air Transport Association (IATA) (2016), *Annual Review*.

Jazar, R.N. (2008), *Vehicle Dynamics: Theory and Applications*, Springer, New York, U.S.A.

Kerrebrock, J.L. (1992), *Aircraft Engines and Gas Turbines*, 2nd Edition, MIT Press, Cambridge, U.S.A.

Kuznetsov, V.M. (2003), "Noise control problems of passenger airplanes (a review)", *Acoust. Phys.*, **49**(3), 241-262.

Larminie, J. and Lowry, J. (2012), *Electric Vehicle Technology Explained*, 2nd Edition, John Wiley & Sons, Chichester, West Sussex, U.K.

Mair, W.A. and Birdsall, D.L. (1992), *Aircraft Performance*, Cambridge University Press, Cambridge, U.K.

Mattingly, J.D. (2005), *Elements of Gas Turbine Propulsion*, American Institute for Aeronautics and Astronautics (AIAA), Reston, Virginia, U.S.A.

McCormick, B.W. (1995), *Aerodynamics, Aeronautics and Flight Mechanics*, 2nd Edition, John Wiley & Sons, New York, U.S.A.

Miller, J.M. (2004), *Propulsion Systems for Hybrid Vehicles*, IEEE, London, U.K.

Milliken, W.F. and Milliken, D.L. (1995), *Race Car Vehicle Dynamics*, Society of Automotive Engineers International (SAE), Warrendale, Pennsylvania, U.S.A.

Mirosavljević, P., Gvozdenović, S. and Čokorilo, O. (2011), "A model of air traffic assignment as part of airport air pollution management system", *Aviat.*, **15**(4), 92-100.

Moir, I. and Seabridge, A. (2008), *Aircraft Systems-Mechanical, Electrical, and Avionics Subsystems Integration*, 3rd Edition, John Wiley and Sons, Chichester, U.K.

Moir, I. and Seabridge, A. (2013), *Design and Development of Aircraft Systems*, 2nd Edition, John Wiley & Sons, New York, U.S.A.

Morlok, E.K. (1978), *Introduction to Transportation Engineering and Planning*, McGraw-Hill, New York, U.S.A.

Nicolai, L.M. and Carichner, G.E. (2010), *Fundamentals of Aircraft and Airship Design: Volume I-Aircraft Design*, American Institute for Aeronautics and Astronautics (AIAA), Reston, Virginia, U.S.A.

Page, J. and Hobbs, C. (2010). "Modeling of noise from aircraft taxiing operations", *J. Acoust. Soc. Am.*, **127**, 1834.
Raymer, D.P. (1999), *Aircraft Design: A Conceptual Approach*, 3rd Edition, American Institute for Aeronautics and Astronautics, Reston, Virginia, U.S.A.
Roskam, J. and Lan, C.T. (1997), *Airplane Aerodynamics and Performance*, DAR Corporation, Lawrence, U.S.A.
Scholz, D., Seresinhe, R., Staack, I. and Lawson, C. (2013), "Fuel consumption due to shaft power off-takes from the engine", Workshop on Aircraft System Technologies, Hamburg, Germany, April.
Stansfeld, S. (2013), "Airport noise and cardiovascular disease", *BMJ*, **347**.
Swatton, P.J. (2008), *Aircraft Performance: Theory and Practice for Pilots*, 2nd Edition, John Wiley & Sons Chichester, U.K.
Teo, A., Rajashekara, K., Hill, J. and Simmers, B. (2008), "Examination of aircraft electric wheel drive taxiing concept", *SAE Technical Paper*, 2008-01-2860.
Treager, I.E. (1995), *Aircraft Gas Turbine Engine Technology*, 3rd Edition, Glencoe McGraw-Hill, New York, U.S.A.
US Department of Transportation, Federal Aviation Administration (2013), *Part 25, Airworthiness Standards: Transport Category Airplanes*, Washington, U.S.A.
US Department of Transportation, Federal Aviation Administration (2014), *Airport Design (AC 150/5300-13A)*, Washington, U.S.A.
Vanker, S., Enneveer, M. and Rammul, I. (2009), "Noise assessment and mitigation schemes for estonian airports", *Aviat.*, **13**(1), 17-25.
Vinh, N.X. (1993), *Flight Mechanics of High-Performance Aircraft*, Cambridge University Press, Cambridge, U.K.
Wild, T.W. (2008), *Transport Category Aircraft Systems*, 3rd Edition, Jeppesen, Englewood, U.S.A.
Wong, J.Y. (2008), *Theory of Ground Vehicles*, 4th Edition, John Wiley & Sons, New York, U.S.A.
Yager, T. (1990), "Tire/runway friction interface", *SAE Technical Paper*, #901912.

EC

Nomenclature

Symbols

A	Work (J or Nm)
b	Wingspan (m)
C_D	Coefficient of Drag, COD (-)
C_L	Coefficient of Lift, COF (-)
D	Drag (N)
e	Oswald efficiency factor (aerodynamics)
g	Terrestrial gravitational acceleration (m/s^2)
h	Height (m)

i	Transmission/Gear ratio (-)
I	Mass moment of rotational inertia (kg m^2)
K	Drag-due-to-lift coefficient (-)
L	Lift (N)
$\dot{m}$	Mass flow rate (kg/s)
M	Mass (kg)
M	Mach number (-)
N	Angular speed (RPM)
P	Power (W)
r	Radius (m)
s	Distance (m)
S	Surface area (airplane reference area) (m^2, ft^2)
t	Time (s)
T	Thrust (N)
v	Velocity (vector), speed (scalar) (m/s, knot)
W	Weight (N)

Greek

α	Angle-of-Attack (AOA) (rad)
β	IGE influence factor (-)
η	Coefficient of efficiency (-)
κ	Coefficient of added rotational inertia (-)
μ	Friction coefficient (-)
ρ	Mass density (kg/m^3)
τ	Torque (Nm)

ω	Angular speed (rad/s)
ϕ	Surface slope (rad)

Subscripts

A	Airplane, Aircraft
eff	Effective
f	Fuel
ref	Reference
tract	Tractive
w	Wind
wet	Wet (surface, surface area)

Abbreviations

AC	Alternating Current
AOA	Angle of Attack
APU	Auxiliary Power Unit (turboshaft, aircraft)
AR	Aspect Ratio (-)
BLDC	Brushless DC (electric motor)
CAA	Civil Aviation Authority (UK)
CF	Constant Frequency
CG	Center of Gravity
CM	Center of Mass
CRR	Coefficient of Rolling Resistance ((-))
CS	Certification Specifications (EASA)
CTF	Coefficient of Tractive Friction ((-))
DC	Direct Current

EASA	European Aviation Safety Agency
ETOPS	Extended Operations and Polar Operations (FAA)
FAA	Federal Aviation Administration (US)
FAR	Federal Aviation Regulations (FAA)
FC	Fuel Consumption
FL	Flight Level
GA	General Aviation
GBX	Gearbox (transmission)
GS	Groundspeed (m/s, km/hr, knot)
HBPR	High Bypass-Ratio (jet/turbofan engine)
HC	Hydrocarbon (fuels)
HP	Horse-power (non-SI unit of power 0.746 kW)
HW	Headwind
IATA	International Air Transportation Association
ICAO	International Civil Aviation Organization (UN age ncy)
IGBT	Insulated Gate Bipolar Transistor (electronics)
IGE	In-Ground Effect
ISA	International Standard Atmosphere
LHV	Lower Heating Value (thermodynamics) (kJ/kg)
LIB	Lithium-Ion Batteries (electrical)
MAC	Mean Aerodynamic Chord
MEA	More Electric Airplane
MFD	Multi-Functional Display
MG	Main (wing or body) Gear

MOSFET	Metal-Oxide-Semiconductor Field-Effect Transistor (electronics)
MRW	Maximum Ramp/Taxi Weight (aircraft)
MTOW	Maximum Take-Off Weight (aircraft)
NG	Nose Gear
NM	Nautical mile (=1.852 km)
RB	Regenerative Braking
RPM	Revolutions per Minute
RWY	Runway (airport)
SFC	Specific Fuel Consumption (jet engine)
SL	Sea-Level
SRM	Switched Reluctance Machine/Motor (electrical)
TSFC	Thrust Specific Fuel Consumption (jet engine)
TW	Tailwind
TWY	Taxiway (airport)
UHBPR	Ultra-High Bypass-Ratio (jet/turbofan engine)
VA	Volt-Ampere (unit of apparent electric power)
VAC	Volts AC
VSCF	Variable Speed Constant Frequency